

# The Megamaser Cosmology Project. X. High Resolution Maps and Mass Constraint for SMBHs

W. Zhao<sup>1,2</sup>, J. A. Braatz<sup>3</sup>, J. J. Condon<sup>3</sup>, K. Y. Lo<sup>3</sup>, M. J. Reid<sup>4</sup>, C. Henkel<sup>5,6</sup>, D. W. Pesce<sup>7</sup>, J. E. Greene<sup>8</sup>, F. Gao<sup>3,9,10</sup>, C. Y. Kuo<sup>11</sup>, and C. M. V. Impellizzeri<sup>3,12</sup>

<sup>1</sup>*Shanghai Observatory, 80 Nandan Road, Shanghai 200030, China*

<sup>2</sup>*Key Laboratory of Radio Astronomy, Chinese Academy of Sciences, 210008 Nanjing, PR China*

<sup>3</sup>*National Radio Astronomy Observatory, 520 Edgemont Road, Charlottesville, VA 22903, USA*

<sup>4</sup>*Harvard-Smithsonian Center for Astrophysics, 60 Garden Street, Cambridge, MA 02138, USA*

<sup>5</sup>*Max-Planck-Institut für Radioastronomie, Auf dem Hügel 69, 53121 Bonn, Germany*

<sup>6</sup>*King Abdulaziz University, P.O. Box 80203, Jeddah, Saudi Arabia*

<sup>7</sup>*Department of Astronomy, University of Virginia, Charlottesville, VA 22904*

<sup>8</sup>*Department of Astrophysical Sciences, Princeton University, Princeton, NJ 08544, USA*

<sup>9</sup>*Key Laboratory for Research in Galaxies and Cosmology, Shanghai Astronomical Observatory, Chinese Academy of Science, Shanghai 200030, China*

<sup>10</sup>*Graduate School of the Chinese Academy of Sciences, Beijing 100039, China*

<sup>11</sup>*Department of Physics, National Sun Yat-Sen University, No.70, Lianhai Rd., Gushan Dist., Kaohsiung City 804, Taiwan (R.O.C.)*

<sup>12</sup>*Joint Alma Office, Alonso de Cordova 3107, Vitacura, Santiago, Chile*

## ABSTRACT

We present high resolution (sub-mas) VLBI maps of nuclear H<sub>2</sub>O megamasers for seven galaxies. In UGC 6093, the well-aligned systemic masers and high-velocity masers originate in an edge-on, flat disk and we determine the mass of the central SMBH to be  $M_{\text{SMBH}} = 2.58 \times 10^7 M_{\odot}$  ( $\pm 7\%$ ). For J1346+5228, the distribution of masers is consistent with a disk, but the faint high-velocity masers are only marginally detected, and we constrain the mass of the SMBH to be in the range  $1.5 - 2.0 \times 10^7 M_{\odot}$ . The origin of the masers in Mrk 1210 is less clear, as the systemic and high-velocity masers are misaligned and show a disorganized velocity structure. We present one possible model in which the masers originate in a tilted, warped disk, but we do not rule out the possibility of other explanations including outflow masers. In NGC 6926, we detect a set of redshifted masers, clustered within a pc of each other, and a single blueshifted

maser about 4.4 pc away, an offset that would be unusually large for a maser disk system. Nevertheless, if it is a disk system, we estimate the enclosed mass to be  $M_{\text{SMBH}} < 4.8 \times 10^7 M_{\odot}$ . For NGC 5793, we detect redshifted masers spaced about 1.4 pc from a clustered set of blueshifted features. The orientation of the structure supports a disk scenario as suggested by Hagiwara et al. (2001). We estimate the enclosed mass to be  $M_{\text{SMBH}} < 1.3 \times 10^7 M_{\odot}$ . For NGC 2824 and J0350–0127, the masers may be associated with pc or sub-pc scale jets or outflows.

## 1. Introduction

H<sub>2</sub>O megamasers are found in high-density, warm molecular gas with a large water abundance in the central parsec of galaxies with Seyfert 2 or LINER spectra, either in **the circumnuclear disks**, or associated with the jets and outflows triggered by these active galactic nuclei (AGNs). **In the circumnuclear disks**, the masing gas is heated by X-ray irradiation or shocks and viscosity within the disk (Neufeld et al. 1994). In the jets and outflows impacting the surrounding molecular clouds, the maser emission arises in the post-shock gas (Lo 2005).

The Megamaser Cosmology Project has the primary goal of measuring the Hubble Constant,  $H_0$ , by determining angular diameter distances to circumnuclear megamasers in AGNs well into the Hubble flow (Reid et al. 2009; Braatz et al. 2010; Reid et al. 2013; Kuo et al. 2013; Gao et al. 2016). A second important goal of the project is to measure precise masses of the supermassive black holes (SMBHs) in the nuclei of these galaxies. Very Long Baseline Interferometry (VLBI) provides both the sub-milliarcsecond angular resolution needed to map the extremely compact masing regions and the spectral resolution needed to study their kinematics. VLBI can resolve the gravitational “sphere of influence” of the SMBH in many megamaser disks, and the mass can be measured accurately when the rotation of the edge-on disk is observed to be Keplerian. **To date, with this method, 20 SMBH masses have been measured (e.g. Greenhill et al. 1996; Herrnstein et al. 1999; Greenhill et al. 2003; Kondratko et al. 2005, 2008; Reid et al. 2009; Kuo et al. 2011; Yamauchi et al. 2012; Gao et al. 2016; Greene et al. 2016a; Gao et al. 2017.)** Most of the measured values are between  $10^6$  and a few times of  $10^7 M_{\odot}$ , and the extremely high mass densities ( $\rho \gtrsim 10^{11} M_{\odot} \text{ pc}^{-3}$ ) inside the maser disks argue strongly against alternatives to SMBHs (e.g., a dense cluster of stars or stellar remnants) as the central objects in these galaxies. The “gold standard” SMBH masses measured with megamasers provide a strong test of the  $M_{\text{SMBH}}-\sigma_{\star}$  relation at its low-mass end (Ferrarese & Merritt 2000; Gebhardt et al. 2000; Gültekin et al. 2009; Kormendy & Bender 2011; Kormendy et al. 2011; Greene 2012; Greene et al. 2016a,b).

Although edge-on disk masers in Keplerian rotation are the best-studied class of megamasers, not all megamaser sources originate from such systems. Some megamasers form in non-Keplerian disks, and some show complex geometries influenced by nuclear jets and outflows. Still other megamasers have single-dish spectral profiles with hints of disk emission, such as high-velocity

components, but their VLBI maps reveal complex geometries and disordered dynamics. In these cases, SMBH masses can not be determined simply by fitting a Keplerian rotation curve.

In this paper, we present VLBI images of megamasers whose single-dish spectral profiles show a range of properties. One has the characteristic triple-peaked disk profile (UGC 6093). Others have asymmetric high-velocity maser components, or broad systemic components with no apparent high-velocity counterparts. We determine an accurate SMBH mass for UGC 6093 by fitting a disk model to the observed maser components. For other systems with high-velocity components, we apply other methods to determine constraints on the enclosed mass, assuming the masers originate in a disk. Our mass estimates for the SMBHs in these megamaser systems are proportional to its distance, which we calculate from the galaxy’s recessional velocity assuming  $H_0 = 70 \text{ km s}^{-1} \text{ Mpc}^{-1}$  (Dunkley et al. 2009).

## 2. The Sample, Observations and Data Reduction

### 2.1. The Megamaser Sample

The seven galaxies presented in this paper are Seyfert 2 galaxies and LINERs, whose  $\text{H}_2\text{O}$  megamasers were discovered between 1994 and 2011. The  $\text{H}_2\text{O}$  masers in UGC 6093, J1346+5228 and J0350–0127 were discovered by the MCP survey with the Green Bank Telescope (GBT), while the remaining masers were discovered in earlier surveys (Braatz et al. 1994; Hagiwara et al. 1997; Greenhill et al. 2003). Table 1 lists the properties (e.g. name, recession velocity referenced to the local standard of rest (LSR), referred to as systemic velocity hereafter, angular size distance when  $H_0 = 70 \text{ km s}^{-1} \text{ Mpc}^{-1}$ , morphology and AGN type) of the galaxies and discovery references. Only NGC 5793 had prior VLBI images, but since only blueshifted masers had been detected (Hagiwara et al. 2001), we re-observed NGC 5793 to image the redshifted and systemic masers to test the “compact molecular disk” model proposed by Hagiwara.

### 2.2. Observations

**We observed all seven galaxies between 2010 May and 2013 January with the Very Long Baseline Array (VLBA) augmented by the Green Bank Telescope (GBT), meanwhile the 100-m Effelsberg (EB) telescope was also used for UGC 6093.** Mrk 1210 and UGC 6093 were observed for three tracks each; the other five galaxies were observed for one track each. Details of the observations are listed in Table 2. The observations were designed to minimize phase errors that could degrade the accuracy of the maser positions: (1) To remove the tropospheric delay and clock errors, we scheduled two “geodetic blocks” with durations of 45–60 minutes and observed in left circular polarization with eight 16 MHz bands spanning 374 to 476 MHz (see the frequency coverage for each VLBI track in Table 2) before and after the “maser blocks” for target galaxies. In each

geodetic block,  $\sim 20$  compact radio sources covering a wide range of zenith angles were observed to estimate vertical tropospheric delays and clock offsets at each antenna. (2) To remove electronic delay differences among intermediate frequency (IF) sub-bands, scans of 5–10 minutes duration on strong compact sources were interspersed between the maser blocks. (3) All megamasers except J1346+5228 were observed in self-calibration mode, where a bright maser spot was used to remove phase variations from the atomic clocks and tropospheric delays (see LSR velocities of the masers used as calibrators in column 8 of Table 2). J1346+5228 was observed in phase-referencing mode, where the telescope pointing was switched between the target maser and a nearby (within  $1^\circ$ ) phase-reference source (**4C +53.28**) every 50 s to provide phase calibration.

### 2.3. Data Reduction

We reduced the data using the NRAO Astronomical Image Processing System (AIPS) following the standard procedures for the MCP project (Reid et al. 2009; Kuo et al. 2011; Reid et al. 2013; Kuo et al. 2013; Gao et al. 2016). Then the calibrated interferometer ( $u, v$ )-data from adjacent VLBI tracks of Mrk 1210 (BK163A and BK163C, referred as BK163AC and considered as one track hereafter) and UGC 6093 (BB294C and BB294E, referred as BB294CE and considered as one track hereafter) were combined for better sensitivity. Next, we spectrally smoothed the calibrated data to 125 kHz ( $\sim 1.8 \text{ km s}^{-1}$ ) per channel, then constructed images by Fourier transformed and CLEANing with the AIPS task IMAGR. Columns 5 and 6 of Table 2 list the synthesized half-power beamwidths, position angles, and rms sensitivities of these images. We fit elliptical Gaussians to the detected maser features to obtain their positions and peak flux densities. Table 3 shows a sample of fitting results for VLBI track BB278I of UGC 6093, including nonrelativistic “optical convention” radial velocities defined by  $V \equiv c(\Delta\lambda/\lambda)$ . We generate spectra from the VLBI cubes to compare with single-dish spectra. The VLBI spectra were produced by using the fitted peak flux densities and velocities of masers with  $\text{SNR} > 3$  (SNR is the ratio of the peak flux density to its rms uncertainty), while using the rms noise of the CLEANed VLBI image as the noise level of the spectra.

To make the maser maps, we determined the position offsets of masers with  $\text{SNR} > 5$  relative to the brightest systemic maser, except in the case of NGC 5793 where we measured offsets relative to the brightest redshifted maser. For UGC 6093, to refine the VLBI map and show the emission structure more clearly, we grouped the masers detected in its VLBI spectra into clumps, and averaged the data in the velocity range (see the velocity range of each clump detected in VLBI track BB278I in Table 4, and see the velocity range of each clump detected in BB294CE in on-line Table 4.1) of each clump spectrally to increase the SNR and thus decrease the position error. Then we Fourier transformed, CLEANed and fitted the re-averaged data (see the fitting results of re-averaged data of VLBI track BB278I in Table 4, as well as fitting results of re-averaged data in BB294CE in on-line Table 4.1). We referred positions of masers detected in VLBI track BB278I and BB294CE to the masers in the velocity range  $10834.67\text{--}10850.07 \text{ km s}^{-1}$  and  $10814.30\text{--}10850.52 \text{ km s}^{-1}$  respectively,

and finally made a single map by aligning the positions of those two masers. Mrk 1210 also has two VLBI data sets (BB313B and BK163AC). We first referred positions of masers detected in both of them to the maser at velocity  $4227.84 \text{ km s}^{-1}$ , then made a single map by aligning the positions of the reference maser, and finally moved the map center to the position of the only systemic maser. For J1346+5228, to refine the VLBI map, we spectrally smoothed data containing systemic masers to  $500 \text{ kHz}$  ( $\sim 7.2 \text{ km s}^{-1}$ ) per channel, and averaged channels containing red and blueshifted masers into two channels respectively (see the velocity range we used to average the data in on-line Table 4.1). We produced the final map of J1346+5228 with the re-averaged data (see the fitting results of re-averaged data of VLBI track BB313X in online Table 4.1).

### 3. VLBI Spectra and maps of $\text{H}_2\text{O}$ Megamasers

As mentioned in Section 2.3, we compared the VLBI spectra with quasi-simultaneous high-sensitivity ( $\sigma \sim 3 \text{ mJy beam}^{-1}$ ) GBT spectra in Figure 1. For Mrk 1210 and UGC 6093, the most sensitive VLBI tracks (BB313B and BB278I for Mrk 1210 and UGC 6093 respectively) were used in this comparison. Almost all maser features from the single-dish spectra are detected in our VLBI observations, except for one blueshifted maser and a small fraction of redshifted masers in NGC 6926, and one redshifted maser in NGC 5793. The VLBI flux densities of most masers agree well with the single-dish observations. The differences between the VLBI and single-dish flux densities of some individual lines can mainly be attributed to maser variability.

UGC 6093 has been monitored occasionally by the MCP with the GBT since 2007. The upper left panel of Figure 1 compares the VLBI spectrum with a GBT spectrum taken four months earlier, on 2009 December 1. UGC 6093 has the characteristic triple-peaked spectrum of a disk maser. Compared to other disk maser systems, the red and blue-shifted masers span relatively narrow velocity windows of  $74 \text{ km s}^{-1}$  and  $92 \text{ km s}^{-1}$ , respectively. The upper-right panel of Figure 1 displays single-dish spectra of the systemic masers from four epochs, showing that the systemic masers are quite variable.

Mrk 1210 has been monitored with the GBT periodically since 2003. The bottom left panel of Figure 1 shows the GBT spectrum taken on 2012 January 25 compared with the VLBI spectrum taken 11 days later. While Mrk 1210 does not have the characteristic triple-peaked spectrum of a disk maser, the spectrum does show a large overall range of detected velocities covering  $\sim 600 \text{ km s}^{-1}$ , bracketing the systemic velocity, and thus suggestive of high-velocity rotation around a SMBH. The redshifted maser detected near  $4228 \text{ km s}^{-1}$  with a width of  $\sim 3 \text{ km s}^{-1}$  was flaring at the time of the observations. The weak near-systemic maser at  $4088 \text{ km s}^{-1}$  with a width of  $1.7 \text{ km s}^{-1}$  only appeared for a short period in early 2012. The bottom right panel of Figure 1 displays single-dish spectra on the flaring maser feature at four epochs. The peak flux density varied from  $0.19 \text{ Jy beam}^{-1}$  to nearly  $0.5 \text{ Jy beam}^{-1}$  within two years, while weaker high-velocity masers were relatively stable.

J1346+5228 (Figure 2) has the typical triple-peaked spectrum of disk masers, but the high-velocity masers are barely detectable at flux densities  $< 10$  mJy. The redshifted masers peaking around  $9478 \text{ km s}^{-1}$  and blueshifted masers peaking around  $7972 \text{ km s}^{-1}$  are symmetrically offset from the systemic velocity by more than  $700 \text{ km s}^{-1}$ , **and cover narrow velocity ranges of  $6 \text{ km s}^{-1}$  and  $9 \text{ km s}^{-1}$  respectively.**

NGC 6926 has a spectrum asymmetric in both velocity and strength (Figure 2). The spectrum shows a very weak feature at  $5912 \text{ km s}^{-1}$  near the systemic velocity and a broad (width  $> 100 \text{ km s}^{-1}$ ) redshifted line complex with flux densities over a few tens of mJy. Two blueshifted features with flux densities of 20 mJy and 15 mJy are detected at  $5775 \text{ km s}^{-1}$  and  $5815 \text{ km s}^{-1}$  in the single-dish spectrum respectively, while only the former one is detected in the VLBI observation.

Hagiwara discovered the  $\text{H}_2\text{O}$  megamaser in NGC 5793 with the Nobeyama 45 m telescope (Hagiwara et al. 1997) and made subsequent interferometric studies (Hagiwara et al. 2001). Single-dish observations made in the 1990s showed a hint of features near the systemic velocity. Blueshifted features were detected  $> 200 \text{ km s}^{-1}$  away from the systemic velocity while redshifted features at  $3677 \text{ km s}^{-1}$  were detected in only one epoch by the Nobeyama 45 m. Our GBT and VLBI spectrum (Figure 2) revealed no detected maser features near the systemic velocity but both the blueshifted and redshifted maser features were detected for the first time in the VLBI observation.

The single-dish and VLBI spectra of both NGC 2824 and J0350–0127 show no high velocity features characteristic of a disk maser. Most of the megamaser emission from NGC 2824 comes from a broad line complex in the velocity range from  $2500$  to  $3000 \text{ km s}^{-1}$  (Figure 2). The broad profile of the spectrum of NGC 2824 is similar to those of NGC 1052 and Mrk 348, in which the masers originate from the pc-scale nuclear jet (Claussen et al. 1998; Falcke et al. 2000; Peck et al. 2003). In J0350–0127, the masers are confined to a narrow velocity range between  $12320$  and  $12380 \text{ km s}^{-1}$  and peak at  $12352 \text{ km s}^{-1}$ , only  $45 \text{ km s}^{-1}$  from the systemic velocity.

### 3.1. UGC 6093

The VLBI map of UGC 6093 (Figure 3) reveals an edge-on disk. The well-aligned systemic masers and high-velocity masers define a disk plane with little or no warping. The redshifted side of the disk plane has a position angle  $PA \sim -20^\circ$  east of north (this definition of position angle  $PA$  is kept in the following subsections). The diameter of the disk is about  $0.9 \text{ mas}$  or  $\approx 0.6 \text{ pc}$ , which is within the typical range of sizes for megamaser disks.

We used a Bayesian fitting program (Reid et al. 2013) to estimate the mass of the central black hole in UGC 6093. The program was originally used to estimate the Hubble constant for MCP galaxies. By fitting the positions, radial velocities (with relativistic corrections), and accelerations (measured by monitoring velocity shifts of the systemic maser features) of masers, this program estimates the positions of masers in the disk plane and gives best-fit values for the mass and

position of the SMBH, recession velocity of the SMBH, and the Hubble constant (an angular-size distance can be inferred from the latter two parameters).

We monitored the maser spectrum of UGC 6093 periodically with the GBT over nine years, but the systemic lines were too variable and blended to track velocity drifts reliably from epoch to epoch. So the maser in UGC 6093 is not well suited to a distance measurement for the MCP. Nevertheless, we can still apply the full 3D fitting program to measure the BH mass based on an adopted value of Hubble constant  $H_0 = 70 \text{ km s}^{-1} \text{ Mpc}^{-1}$ . We fit a flat disk because the VLBI map does not reveal a warp in a convincing way. We also fit circular orbits, since in previous MCP work (Reid et al. 2013; Kuo et al. 2013; Gao et al. 2016), any eccentricity for maser feature orbits turned out to be very small. So six parameters remained to be fit: three for the position and mass of the SMBH (the right ascension  $x_0$ , declination  $y_0$ , and mass  $M_{\text{SMBH}}$ ), two for the geometry of the disk (position angle  $PA$  and inclination angle  $i$ ), and one for the recession velocity referenced to the LSR ( $v_{\text{LSR}}$ ). We use only maser features with  $\text{SNR} > 7$ . Since we did not have reliable acceleration, we adopted nominal acceleration values with large uncertainties ( $4 \pm 50 \text{ km s}^{-1} \text{ yr}^{-1}$ ). The fit, then, is still constrained in part by the measured positions of those maser spots, since the mass measurement is almost free from the value of acceleration even removing the systemic features from the fit produced no significant changes to the black hole mass estimate.

We list the most likely parameter values and the 68% confidence ranges derived from Bayesian fitting for UGC 6093 in the first line of Table 5 and show the fitting results graphically in Figure 5. Marginalized probability density functions (PDFs) of the parameters (generated by binning the the MCMC trials) are presented in the upper left panel. These PDFs appear smooth and symmetric for all parameters. The upper right panel is a top view of the maser disk, showing the best-fit maser positions. The lower left panel shows the 3-D disk model superposed with masers as seen on the sky. The lower right panel presents the  $PV$  diagram. The dashed line presents the position-velocity relation in an ideal case, an edge-on, flat, Keplerian disk orbiting around a point mass with our fitted value. As the figure shows, data points of UGC 6093 slightly deviate from the ideal model.

The distance from the masers to the SMBH ranges between 0.17 and 0.33 mas (0.12 to 0.24 pc). Almost all of the high-velocity masers are located along the mid-line of the disk as is common for disk megamasers. The 3-D geometric model (an edge-on disk at inclination angle  $i = 93.8^\circ$  and position angle  $PA = -20.1^\circ$ ) constrained by our observations is a good fit. The SMBH lies within 0.01 mas of the reference center of the VLBI map, and the fitted mass is  $M_{\text{SMBH}} = 2.58^{+0.11}_{-0.09} \times 10^7 M_\odot$ . For the black hole mass, in addition to the formal fitting error ( $\sim 3.8\%$ ) there are two main sources of systemic error: **(1) Uncertainty in the distance to the galaxy. In this paper, we adopted  $H_0 = 70 \text{ km s}^{-1} \text{ Mpc}^{-1}$  with an uncertainty of 5% ( $\sigma_1$ ). This uncertainty will pass down to the mass, which is proportional to  $H_0$ . (2) Uncertainty in the absolute positions for the reference maser spots, which are  $\sim 10 \text{ mas}$  based on Very Large Array measurements; for self-calibrated VLBI observations, this position uncertainty introduces an error up to 5% ( $\sigma_2$ ) in the SMBH mass (Kuo et al. 2011). Combining these sources of systematic uncertainty, we estimate a total systematic uncertainty in the SMBH mass of  $\sqrt{\sigma_1^2 + \sigma_2^2} \sim 7\%$ .** The best fit LSR recession velocity of

the SMBH is  $v_{\text{LSR}} = 10621^{+11}_{-12} \text{ km s}^{-1}$ . An angular-size distance  $d_A = 151.7 \text{ Mpc}$  can be inferred from the velocity of the SMBH and our adopted Hubble constant. But we do not know the exact value of angular-size distance to UGC 6093, so specifying  $M_{\text{SMBH}}$  in terms of  $D_A$  is a good compromise. Since our  $M_{\text{SMBH}}$  estimates are directly proportional to the angular-size distance, the mass can be expressed as  $M_{\text{SMBH}} = 2.58 \times 10^7 \left( \frac{D_A}{151.7 \text{ Mpc}} \right) M_{\odot}$ .

### 3.2. Mrk 1210

The Mrk 1210 VLBI map in Figure 3 shows redshifted and blueshifted maser features in separate clusters separated by 7 mas or  $\approx 2 \text{ pc}$ , with a  $PA \sim -120^\circ$ . A single maser component detected near the systemic velocity falls between the two clusters but offset from the connecting line. While the general configuration of maser features is roughly consistent with disk rotation, the exact nature of the maser system remains inconclusive. If indeed that masers arise in a disk, the misalignment of the maser features suggests the potential of warping or eccentricity in the disk, or an inclination different from edge-on. The left panel of Figure 6 shows a concept map of a warped and tilted disk overlapping with the observed masers with  $\text{SNR} > 7$  in Mrk 1210.

Assuming a disk origin and approximating the radius as half the full extent of the megamaser emission, and the rotation velocity as the velocity offset of the high-velocity masers from the systemic velocity, we estimated the mass enclosed within each high-velocity maser component. These values are distributed over a wide range from 0.2 to  $2.2 \times 10^7 M_{\odot}$ . We also tried to estimate the SMBH mass using the same 3-D model fitting method that we applied to UGC 6093. Some parameters (e.g.  $x_0$  and  $y_0$ ) did not converge in the attempted fit, implying the present data do not adequately constrain the assumed model. We consider a representative value for the SMBH mass ( $1.42 \times 10^7 M_{\odot}$ ), which we use for reference only in Figure 6 and Table 5. The dashed line in the right panel of Figure 6 presents the  $PV$  relation of an edge-on, flat, Keplerian disk orbiting a point mass with the reference value. Most masers, especially the red-shifted ones with velocities below  $4400 \text{ km s}^{-1}$  and including the flaring feature detected around  $4228 \text{ km s}^{-1}$ , obviously deviate from the fit. These deviations represent unmodeled complexity in this maser system.

### 3.3. J1346+5228

In the VLBI map for J1346+5228 (Figure 3), the high-velocity masers are only marginally detected ( $5\sigma$  for the redshifted and  $4\sigma$  for the blueshifted maser). The distribution of masers is consistent with a disk of diameter 0.5 mas or  $\approx 0.3 \text{ pc}$ . Applying the “edge-on” disk assumption, we defined the line going through the red and blue points as the disk plane, with position angle  $PA \approx 79.2^\circ$ . We also approximated the location of the dynamic center as the unweighted average position of the six systemic masers. The offsets between the projected positions of masers and the



dynamic center on the disk plane are defined as the “impact parameters”. These impact parameters and maser velocities with both special and general relativistic corrections were adopted to produce the  $PV$  diagram shown in Figure 7.

We made two mass estimates for J1346+5228: (1) We used the impact parameters of the redshifted maser (0.24 mas  $\approx$  0.14 pc) and the blueshifted maser (0.22 mas  $\approx$  0.13 pc) and their velocity offsets from the recession velocity  $V_{\text{LSR}}$  to estimate the enclosed mass. The results are  $1.5 \times 10^7 M_{\odot}$  and  $2.0 \times 10^7 M_{\odot}$ , respectively. (2) We noticed that five of the six systemic masers line up well on the  $PV$  diagram (see the enlarged inset in Figure 7), indicating that they form at a common radius from the dynamical center. For a flat edge-on Keplerian disk, the ratio of  $P$  to  $V$  is the orbital angular velocity  $\omega$ . A linear fit to the  $PV$  diagram of the five systemic masers yields  $\omega \approx 5191 \text{ km s}^{-1} \text{ mas}^{-1}$ . If we assume that the radial distance  $r$  of the five systemic masers from the SMBH is about the same as the radius to the high-velocity masers, the enclosed mass  $M = \omega^2 r^3 G^{-1}$  is between  $1.5$  and  $1.9 \times 10^7 M_{\odot}$ . This is within the range of masses enclosed by the high-velocity masers, adding confidence to our estimate that the SMBH in J1346+5228 is between  $1.5 \times 10^7 M_{\odot}$  and  $2.0 \times 10^7 M_{\odot}$ .

### 3.4. NGC 6926

The VLBI map for NGC 6926 in Figure 3 reveals a complex, bent geometry. The redshifted maser complex appears on the map as a cluster with no organized velocity structure. We do not detect any masers with radial velocities  $> 6192 \text{ km s}^{-1}$ . Only one blueshifted maser at  $5775 \text{ km s}^{-1}$  was detected in the VLBI map, while the other at  $5815 \text{ km s}^{-1}$  seen in the GBT spectrum 10 days earlier than the VLBI observation was not detected. The position of the weak systemic maser is closer to the blueshifted maser than to the redshifted masers. This is unexpected since, as the VLBI and single-dish spectrum shows, redshifted masers have greater rotation speed than the blueshifted masers. Whether the “systemic” maser is a part of a potential disk maser system is not clear. The extent of the maser spots is about 11 mas or 4.4 pc, which is larger than the typical diameters of other megamaser disks. Although the observations do not clearly identify a disk origin in this case, we still make an estimation of the NGC 6926 SMBH mass based on a flat, edge-on Keplerian-disk assumption. We estimate a disk radius  $r = 2.2 \text{ pc}$  as half the extent of the megamaser emission, and use the largest velocity offset of the high-velocity masers from the systemic velocity ( $309 \text{ km s}^{-1}$  for NGC 6926) as the rotation velocity ( $V_{\text{rot}}$ ) to estimate an upper limit to the enclosed mass:

$$M_{\text{SMBH}} \lesssim 4.8 \times 10^7 \left( \frac{r}{2.2 \text{ pc}} \right) \left( \frac{v_{\text{rot}}}{309 \text{ km s}^{-1}} \right)^2 \left( \frac{D_A}{82.2 \text{ Mpc}} \right) M_{\odot} \quad (1)$$

### 3.5. NGC 5793

The multi-epoch VLBI observations of Hagiwara et al. (2001) between 1996 and 1998 detected only the blueshifted masers distributed in two clusters separated by 0.7 mas, and no discernible velocity structure was found in these clusters. The authors proposed a circumnuclear “compact molecular disk” as a possible origin of the masers based on spectral line observations of H<sub>2</sub>O and other molecules in the nuclear region of NGC 5793, and continuum observations of its pc-scale jets, even without the detection of any redshifted masers.

Our VLBI map in Figure 3 reveals two blueshifted maser clusters, also without any discernible velocity structure. The cluster centered around 3355 km s<sup>−1</sup> (marked with light blue dots) is 0.8 mas away from the other (dark blue). We also detected a redshifted maser at radial velocity 3645 km s<sup>−1</sup> at  $\approx 5.5$  mas northwest of the blueshifted masers. A tentatively-detected 22 GHz continuum source with SNR  $\sim 5$  was detected  $\sim 20$  mas northeast of the maser emission, and it may be a part of the pc-scale jet component C1 mentioned in Hagiwara’s study.

Our redshifted maser was detected at the receding side of the disk, as Hagiwara’s model predicted; our detection thus supports the “disk” scenario as a potential origin of the masers. The positions of the high-velocity masers define a disk plane at position angle  $PA \sim -43^\circ$ . For a flat, edge-on Keplerian-disk with radius of  $r \approx 3$  mas  $\approx 0.7$  pc and rotation velocity  $V \approx 279$  km s<sup>−1</sup>, an upper limit for the enclosed mass is:

$$M_{\text{SMBH}} \lesssim 1.3 \times 10^7 \left( \frac{r}{0.7 \text{ pc}} \right) \left( \frac{v_{\text{rot}}}{279 \text{ km s}^{-1}} \right)^2 \left( \frac{D_A}{49.3 \text{ Mpc}} \right) M_\odot \quad (2)$$

This value is typical for SMBHs in maser galaxies, and it is one order of magnitude lower than the result given in Hagiwara et al. (1997), in which the scale of the disk had been constrained only by the distribution of the 21-cm continuum emission.

### 3.6. NGC 2824 and J0350–0127

On the VLBI map of NGC 2824 (Figure 4), the masers are distributed over an area spanning 20 mas  $\approx 3.8$  pc. Although we do not detect continuum emission in this galaxy, the “broad line” spectral profile is reminiscent of pc-scale jet masers in NGC 1052 and Mrk 348 (Claussen et al. 1998; Falcke et al. 2000; Peck et al. 2003).

For J0350–0127, most of the masers are clustered near the map center, while a few extend to the north by about 0.2 mas  $\approx 0.2$  pc, and others to the west by about 0.5 mas (0.5 pc). The origin of these masers is unclear. They may reveal part of a maser disk, or they may be associated with diffuse outflows.

#### 4. Summary

We present VLBI maps of H<sub>2</sub>O megamasers for seven active galaxies, six for the first time.

The H<sub>2</sub>O megamaser in UGC 6093 clearly originates in a circumnuclear disk orbiting a SMBH of mass  $M_{\text{SMBH}} = 2.58 \times 10^7 M_{\odot}$  ( $\pm 7\%$ ). The H<sub>2</sub>O megamasers in J1346+5228 are also in a disk, but in this case the high-velocity masers are extremely faint. We estimate its SMBH mass lies between  $1.5$  and  $2.0 \times 10^7 M_{\odot}$ .

The maser systems in the other galaxies are complex and have uncertain origins. In Mrk 1210, the spectral profile shows high-velocity components roughly symmetric about the recession velocity of the galaxy. We present a tilted and warped disk as one possible model to describe the maser complex, which extends over about 2 pc. If the masers indeed originate in a disk, the SMBH mass is likely between  $0.2$  and  $2.2 \times 10^7 M_{\odot}$ . The VLBI maps of NGC 6926 and NGC 5793 also reveal emission regions possibly associated with circumnuclear disks. Assuming disk origins, we estimated upper limits to the masses enclosed within the maser disks of  $< 4.8 \times 10^7 M_{\odot}$  for NGC 6926  $< 1.3 \times 10^7 M_{\odot}$  for NGC 5793, Megamasers in the remaining two galaxies, NGC 2824 and J0350–0127, may be associated with  $\sim$  pc-scale jets or outflows.

This research has made use of the NASA/IPAC Extragalactic Database (NED), which is operated by the Jet Propulsion Laboratory, California Institute of Technology, under contract with the National Aeronautics and Space Administration. We thank the referee for helpful comments, and we are grateful to the NRAO VLBA and GBT staff for their many contributions to the Megamaser Cosmology Project. The National Radio Astronomy Observatory is a facility of the National Science Foundation operated under cooperative agreement by Associated Universities, Inc. This work was partially carried out within the Collaborative Research Council 956, subproject A6, funded by the Deutsche Forschungsgemeinschaft (DFG)

*Facilities:* Effelsberg, GBT, VLBA

#### REFERENCES

- Braatz, J. A., Reid, M. J., Humphreys, E. M. L., et al. 2010, ApJ, 718, 657
- Braatz, J. A., Wilson, A. S., & Henkel, C. 1994, ApJL, 437, L99
- Claussen, M. J., Diamond, P. J., Braatz, J. A., Wilson, A. S. & Henkel, C. 1998, ApJL, 500, L129
- Dunkley, J., Spergel, D. N., Komatsu, E., et al. 2009, ApJ, 701, 1804
- Falcke, H., Henkel, Chr., Peck, A. B. et al. 2000, A&A, 358, 17
- Ferrarese, L., & Merritt, D. 2000, ApJL, 539, L9

- Gao, F., Braatz, J. A., Reid, M. J., et al. 2016, *ApJ*, 817, 128
- Gao, F., Braatz, J. A., Reid, M. J., et al. 2017, *ApJ*, 834, 52
- Gebhardt, K., Bender, R., Bower, G., et al. 2000, *ApJL*, 539, L13
- Greene, J., E. 2012, *Nature Communications* 3, 1304
- Greene, J. E., Seth, A., Kim, M., et al. 2016, *ApJL*, 826, L32
- Greene, J. E., Seth, A., Kim, M., et al. 2016, *ApJL*, 832, L26
- Greenhill, L. J., Gwinn, C. R., Antonucci, R., & Barvainis, R. 1996, *ApJL*, 472, L21
- Greenhill, L. J., Booth, R. S., Ellingsen, S. P., et al. 2003, *ApJ*, 590, 162
- Greenhill, L. J., Kondratko, P. T., Lovell, J. E. J., et al. 2003, *ApJL*, 582, L11
- Gültekin, K., Richstone, D. O.; Gebhardt, K., et al. 2009, *ApJ*, 698, 198
- Hagiwara, Y., Kohno, K., Kawabe R., & Nakai, N. 1997, *PASJ*, 49, 171
- Hagiwara, Y., Diamond, P. J., Nakai, N., & Kawabe, R. 2001, *ApJ*, 560, 119
- Herrnstein, J. R., Moran, J. M., Greenhill, L. J., et al. 1999, *Nature*, 400, 539
- Kormendy, J., & Bender, R. 2011, *Nature*, 469, 377
- Kormendy, J., Bender, R., & Cornell, M. E. 2011, *Nature*, 469, 374
- Kondratko, P. T., Greenhill, L. J., & Moran, J. M. 2005, *ApJ*, 618, 618
- Kondratko, P. T., Greenhill, L. J., & Moran, J. M. 2008, *ApJ*, 678, 87
- Kuo, C. Y., Braatz, J. A., Condon, J. J., et al. 2011, *ApJ*, 727, 20
- Kuo, C. Y., Braatz, J. A., Reid, M. J., et al. 2013, *ApJ*, 767, 155
- Lo, K. Y. 2005, *ARA&A* 43, 625
- Neufeld, D. A., Maloney, P. R., & Conger, S. 1994. *ApJL*, 436, L127
- Peck, A. B., Henkel, C., Ulvestad, J. S. et al. 2003, *ApJ*, 590, 149
- Reid, M. J., Braatz, J. A., Condon, J. J., et al. 2009, *ApJ*, 695, 287
- Reid, M. J., Braatz, J. A., Condon, J. J., et al. 2014, *ApJ*, 767, 154
- Yamauchi, A., Nakai, N., Ishihara, Y., Diamond, P., & Sato, N. 2012, *PASJ*, 64, 103

Table 1: The Megamaser Sample

Name	$V_{\text{LSR}}^a$ (km s <sup>-1</sup> )	$D_{\text{A}}^b$ Mpc	Morphology <sup>c</sup>	AGN Type <sup>d</sup>	Discovery Reference
UGC 6093	10800	147.8	SAB(rs)bc	–	MCP, 2007 Dec 30 <sup>e</sup>
Mrk 1210	4032	56.7	S?	Sy	Braatz et al. (1994)
J1346+5228 <sup>f</sup>	8760	120.8	S0	Sy2	MCP, 2006 Dec 12 <sup>e</sup>
NGC 6926	5893	82.2	SB(s)bc pec	Sy2	Greenhill et al. (2003)
NGC 5793	3500	49.3	Sb? edge-on	Sy2	Hagiwara et al. (1997)
NGC 2824	2752	38.9	S0	Sy	Greenhill et al. (2003)
J0350–0127 <sup>g</sup>	12307	167.4	–	–	MCP, 2011 Jan 4 <sup>e</sup>

Notes:

<sup>a</sup> LSR “optical” velocity of host galaxy from the NASA/IPAC Extragalactic Database (NED).

<sup>b</sup> The angular size distance when  $H_0 = 70 \text{ km s}^{-1} \text{ Mpc}^{-1}$ .

<sup>c</sup> Host galaxy morphological type (NED).

<sup>d</sup> AGN type (NED)

<sup>e</sup> Megamaser discovery reference and date.

<sup>f</sup> NED name SBS 1344+527

<sup>g</sup> NED name 2MFGC 03185

Table 2: Observing Parameters

Experiment code	Date	Galaxy	Antennas <sup>a</sup>	Synthesized Beam <sup>b</sup> (mas × mas, deg)	Sensitivity <sup>c</sup> (mJy beam <sup>-1</sup> )	Observing <sup>d</sup> Mode	$V_{ref}^e$ (km s <sup>-1</sup> )	Frequency coverage of geodetic blocks (MHz)
BB278I	2010 Apr 2	UGC 6093	VLBA, GB, EB	1.00×0.29, −11.63	0.84	Self-cal.	10847	21373.49-21781.49
BB294C	2011 Dec 17	UGC 6093	VLBA, GB, EB	1.20×0.25, −15.13 <sup>f</sup>	1.22 <sup>g</sup>	Self-cal.	10838	21373.49-21781.49
BB294E	2012 Jan 29	UGC 6093	VLBA, GB, EB			Self-cal.	10838	21373.49-21781.49
BK163A	2010 May 22	Mrk 1210	VLBA	1.16×0.42, −17.69 <sup>h</sup>	1.25 <sup>i</sup>	Self-cal.	4230	21800.49-22276.49
BK163C	2010 Jul 6	Mrk 1210	VLBA			Self-cal.	4230	21800.49-22276.49
BB313B	2012 Feb 5	Mrk 1210	VLBA, GB <sup>j</sup>	1.26×0.33, −12.24	1.94	Self-cal.	4229	21810.00-22184.00
BB313X	2012 Oct 05	J1346+5228	VLBA, GB	0.64×0.45, +13.95	2.07	Phase-ref <sup>k</sup>	–	21373.49-21781.49
BB313AE	2012 Nov 24	NGC 6926	VLBA, GB	1.26×0.42, −9.42	2.22	Self-cal.	6107	21600.49-21981.49
BB313AI	2012 Dec 17	NGC 5793	VLBA, GB	0.98×0.31, −12.02	3.18	Self-cal.	3230	21810.00-22286.00
BB313AJ	2012 Dec 20	NGC 2824	VLBA, GB	1.53×0.42, −8.29	0.69	Self-cal.	2761	21808.00-22284.00
BB313AL	2013 Jan 02	J0350–0127	VLBA, GB	1.12×0.43, −4.17	1.19	Self-cal.	12351	21308.00-21784.00

Notes:

<sup>a</sup> VLBA: Very Long Baseline Array; GB: Green Bank Telescope of NRAO;

EB: Max-Planck-Institut für Radioastronomie 100m antenna in Effelsberg, Germany.

<sup>b</sup> Except for BB313X, this column shows the restoring beam FWHM size and position angle produced with data averaged over frequency channels used for self-calibration. For BB313X, this column shows the restoring beam FWHM size and position angle (degrees east or north) produced with data averaged over frequency channels that contain the brightest systemic line feature.<sup>c</sup> Except for the galaxy J1346+5228, this column shows the rms noise level of the clean image produced with data averaged over frequency channels used for self-calibration. For BB313X, this column shows the rms noise of the clean image produced with data averaged over frequency channels that contain the brightest systemic line feature.<sup>d</sup> “Self-cal.” means the “self calibration” mode is used.

“Phas-ref.” means the “phase-referencing” mode is used.

<sup>e</sup> LSR velocities of the masers used as calibrators<sup>f</sup> The average restoring beam FWHM size and position angle produced from the data set combined with BB294C and BB294E<sup>g</sup> The sensitivity of the cleaned image produced from the data set combined with BB294C and BB294E <sup>h</sup> The average restoring beam FWHM size and position angle of the image produced from the data set combined with BK163A and BK163C<sup>i</sup> The sensitivity of the cleaned image produced from the data set combined with BK163A and BK163C<sup>j</sup> GB was in the array during the observation but is flagged in data reduction due to its absolute phase instability.<sup>k</sup> The phase-reference source is 4C +53.28.

Table 3: Sample maser fits for UGC 6093 from project BB278I

$V^a$ (km s <sup>-1</sup> )	$\Delta V^a$ (km s <sup>-1</sup> )	$\theta_x^b$ (mas)	$\theta_y^b$ (mas)	$F_v^c$ (mJy beam <sup>-1</sup> )
10859.57	1.82	$-0.0063 \pm 0.0261$	$0.0110 \pm 0.0736$	$3.98 \pm 0.71$
10857.76	1.82	$-0.0098 \pm 0.0133$	$0.0224 \pm 0.0375$	$8.27 \pm 0.75$
10855.95	1.82	$0.0485 \pm 0.0127$	$-0.0789 \pm 0.0358$	$8.77 \pm 0.76$
10854.14	1.82	$-0.0094 \pm 0.0108$	$0.0215 \pm 0.0304$	$10.20 \pm 0.75$
10852.33	1.82	$0.0026 \pm 0.0033$	$-0.0057 \pm 0.0094$	$35.41 \pm 0.80$
10850.52	1.82	$-0.0029 \pm 0.0017$	$-0.0047 \pm 0.0048$	$79.16 \pm 0.92$
10848.71	1.82	$-0.0019 \pm 0.0013$	$-0.0003 \pm 0.0037$	$116.17 \pm 1.05$
10846.89	1.82	$-0.0000 \pm 0.0013$	$0.0000 \pm 0.0037$	$131.71 \pm 1.17$
10845.08	1.82	$-0.0038 \pm 0.0015$	$-0.0001 \pm 0.0042$	$102.13 \pm 1.03$
10843.27	1.82	$0.0012 \pm 0.0020$	$-0.0031 \pm 0.0055$	$72.51 \pm 0.97$
10841.46	1.82	$-0.0038 \pm 0.0024$	$-0.0095 \pm 0.0067$	$53.06 \pm 0.85$
10839.65	1.82	$-0.0016 \pm 0.0033$	$-0.0001 \pm 0.0094$	$35.42 \pm 0.80$
10837.84	1.82	$-0.0013 \pm 0.0040$	$0.0042 \pm 0.0113$	$28.64 \pm 0.78$
10836.03	1.82	$-0.0014 \pm 0.0050$	$0.0092 \pm 0.0140$	$23.47 \pm 0.79$
10834.22	1.82	$0.0173 \pm 0.0095$	$0.0226 \pm 0.0269$	$11.72 \pm 0.76$
10832.41	1.82	$-0.0191 \pm 0.0139$	$-0.0130 \pm 0.0391$	$7.97 \pm 0.75$
10814.30	1.82	$0.0102 \pm 0.0151$	$-0.0558 \pm 0.0427$	$6.88 \pm 0.71$
10812.49	1.82	$-0.0019 \pm 0.0161$	$-0.0497 \pm 0.0455$	$6.61 \pm 0.73$
10810.68	1.82	$-0.0520 \pm 0.0208$	$-0.0459 \pm 0.0587$	$5.31 \pm 0.75$

Notes:

<sup>a</sup> Velocities and channel widths in km s<sup>-1</sup> referenced to the local standard of rest (LSR) and using the nonrelativistic optical velocity convention.

<sup>b</sup> East-west and north-south position offsets from the position of the brightest systemic maser. The listed rms position uncertainties reflect fitting random errors only.

<sup>c</sup> Fitted peak intensity and its rms uncertainty.

Table 4: Re-averaged sample data for UGC 6093

Velocity Range <sup>a</sup> (km s <sup>-1</sup> )	Velocity center <sup>b</sup> (km s <sup>-1</sup> )	$\theta_x$ <sup>c</sup> (mas)	$\theta_y$ <sup>c</sup> (mas)	SNR <sup>d</sup>
11587.18–11615.38	11601.28	$-0.0765 \pm 0.0025$	$0.2410 \pm 0.0068$	57.4
11512.57–11514.38	11513.48	$-0.0871 \pm 0.0145$	$0.2779 \pm 0.0391$	10.0
10834.67–10850.07	10842.37	$-0.0000 \pm 0.0012$	$0.0000 \pm 0.0034$	123.4
10828.33–10832.87	10830.60	$-0.0104 \pm 0.0157$	$-0.0331 \pm 0.0444$	9.4
10109.83–10122.44	10116.14	$0.1197 \pm 0.0055$	$-0.2908 \pm 0.0155$	26.7
10099.02–10107.12	10103.07	$0.1297 \pm 0.0116$	$-0.3251 \pm 0.0329$	12.5
10079.19–10092.71	10085.95	$0.1094 \pm 0.0053$	$-0.2837 \pm 0.0150$	27.6
10048.55–10051.25	10049.90	$0.1251 \pm 0.0177$	$-0.2748 \pm 0.0502$	8.2

Notes:

<sup>a</sup> The range of LSR velocities (optical convention) used for re-averaging.

<sup>b</sup> Center of the velocity range.

<sup>c</sup> East-west and north-south position offsets from the brightest systemic maser. The rms position uncertainties reflect the fitting random errors only.

<sup>d</sup> The ratio of the fitted peak intensity to its rms uncertainty.



Table 5: Bayesian fits for UGC 6093 and Mrk 1210

Galaxy	$M_{\text{SMBH}}^a$ ( $10^7 M_\odot$ )	$x_0^b$ (mas)	$y_0^c$ (mas)	$PA^d$ (deg)	$i^e$ (deg)	$v_{\text{LSR}}^f$ $\text{kms}^{-1}$
UGC 6093	$2.58^{+0.11}_{-0.09}$	$0.009^{+0.008}_{-0.008}$	$0.002^{+0.010}_{-0.009}$	$-20.12^{+1.50}_{-1.65}$	$93.84^{+4.05}_{-3.83}$	$10621.17^{+10.80}_{-12.15}$
Mrk 1210	$1.42^{+0.02}_{-0.02}$	–	–	$-117.42^{+0.45}_{-0.45}$	$100.68^{+1.13}_{-0.90}$	$4007.60^{+3.60}_{-2.25}$

Notes: the values of Mrk 1210 is for reference only.

<sup>a</sup> Mass of the SMBH and its 68% fitting confidence range.

<sup>b</sup> East-west offset of the SMBH from the brightest systemic maser.

<sup>c</sup> North-south offset of the SMBH from the brightest systemic maser.

<sup>d</sup> Position angle of the disk plane (degrees east of north).

<sup>e</sup> Inclination angle between the disk normal and the line of sight.

<sup>f</sup> Optical convention LSR recession velocity.

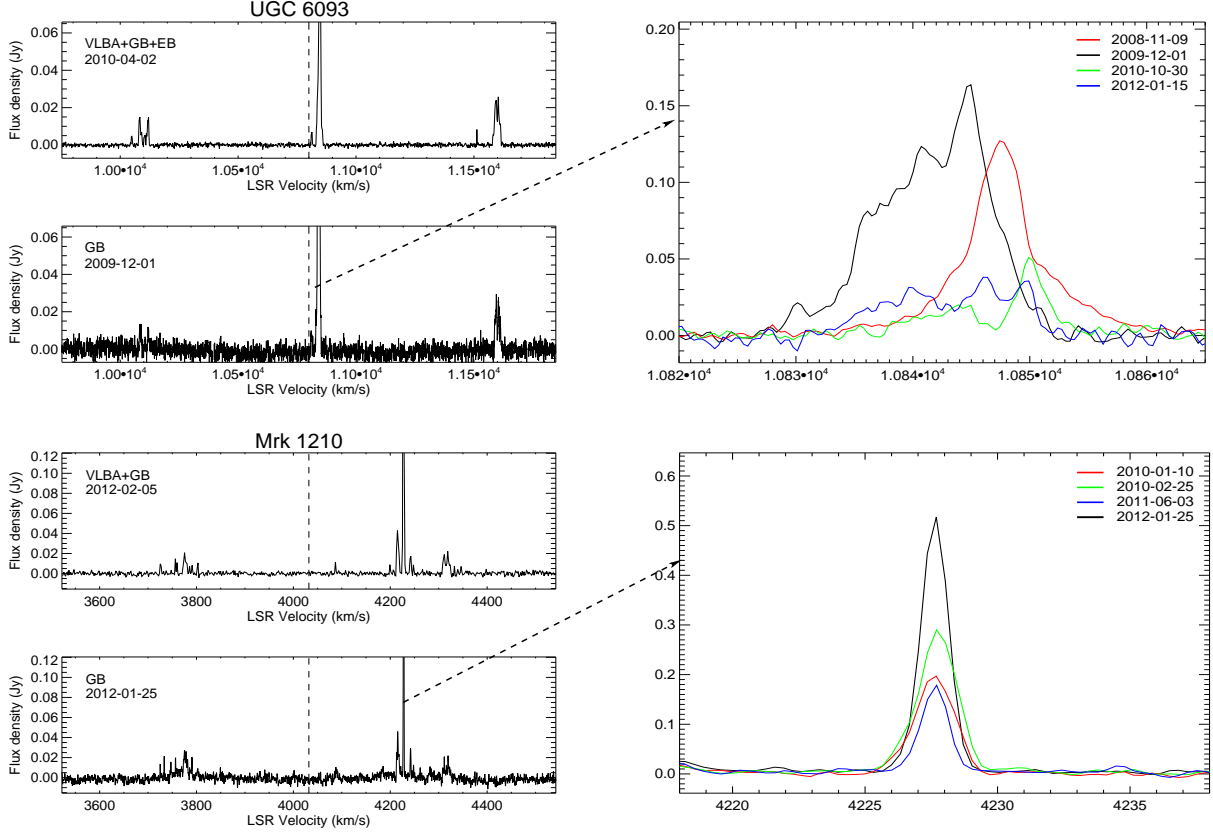


Fig. 1.— The left panels show the VLBI spectra of megamasers in UGC 6093 and Mrk 1210, compared with quasi-simultaneous high-sensitivity ( $\text{rms} \sim 3 \text{ mJy beam}^{-1}$ ) GBT spectra. The vertical dashed lines denote the LSR “optical” velocities of the host galaxies from NED. The right panels present the zoomed-in GBT spectra (black) overlapping three other epochs (colors) during the monitoring period to show the variability of masers in a certain velocity range. For UGC 6093 both the spectral profiles and flux densities of the systemic masers are quite variable; for Mrk 1210, a spectral line at  $4228 \text{ km s}^{-1}$  kept flaring during its GBT monitoring period; e.g., between June 2011 and January 2012 the peak flux density of this maser grew from  $190 \text{ mJy beam}^{-1}$  to nearly  $500 \text{ mJy beam}^{-1}$ .

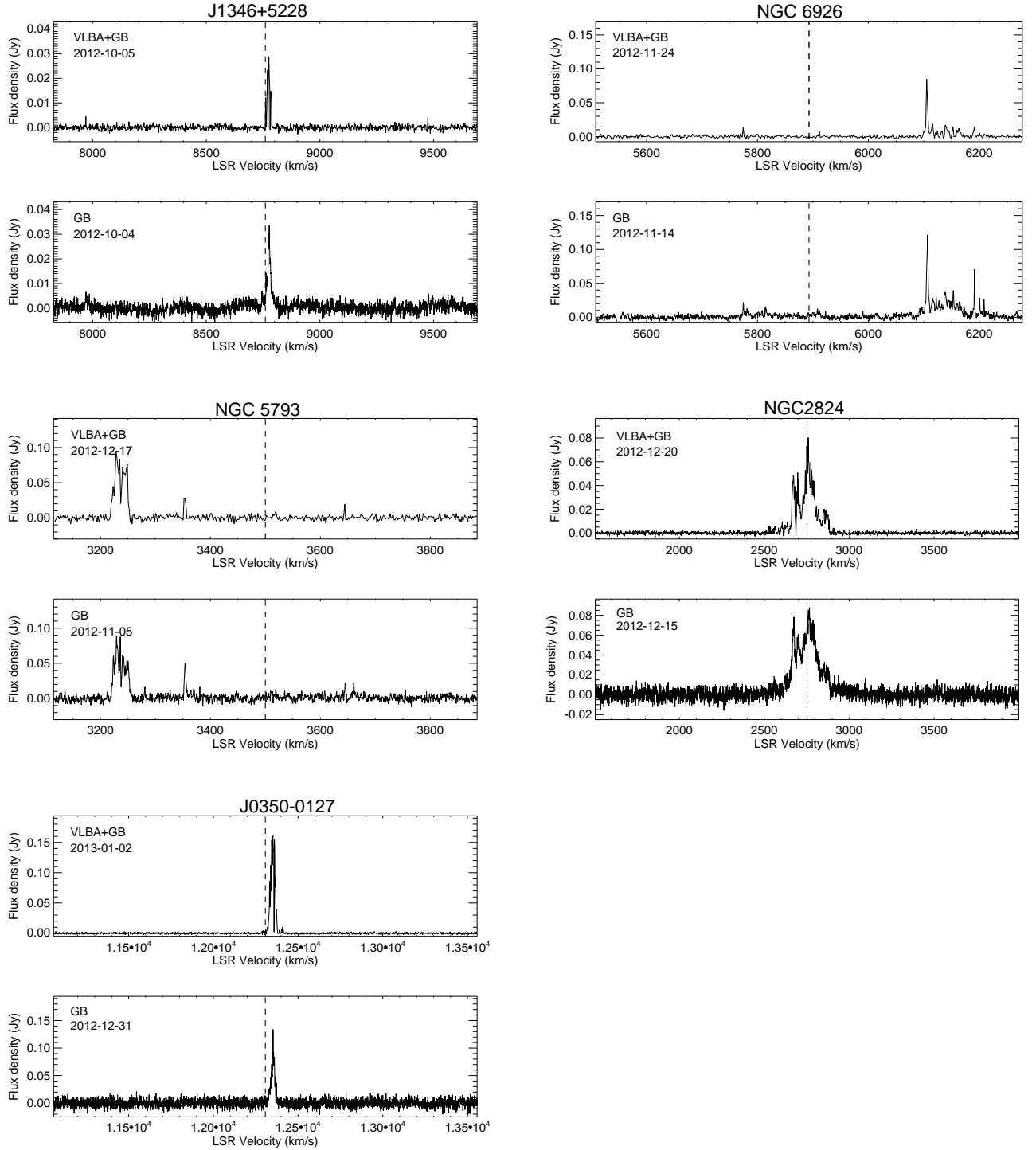


Fig. 2.— VLBI spectra of megamasers in J1346+5228, NGC 6926, NGC 5793, NGC 2824, and J0350–0127 compared with quasi-simultaneous high-sensitivity ( $\text{rms} \sim 3 \text{ mJy beam}^{-1}$ ) GBT spectra. The vertical dashed lines denote the LSR “optical” velocities of the host galaxies from NED.

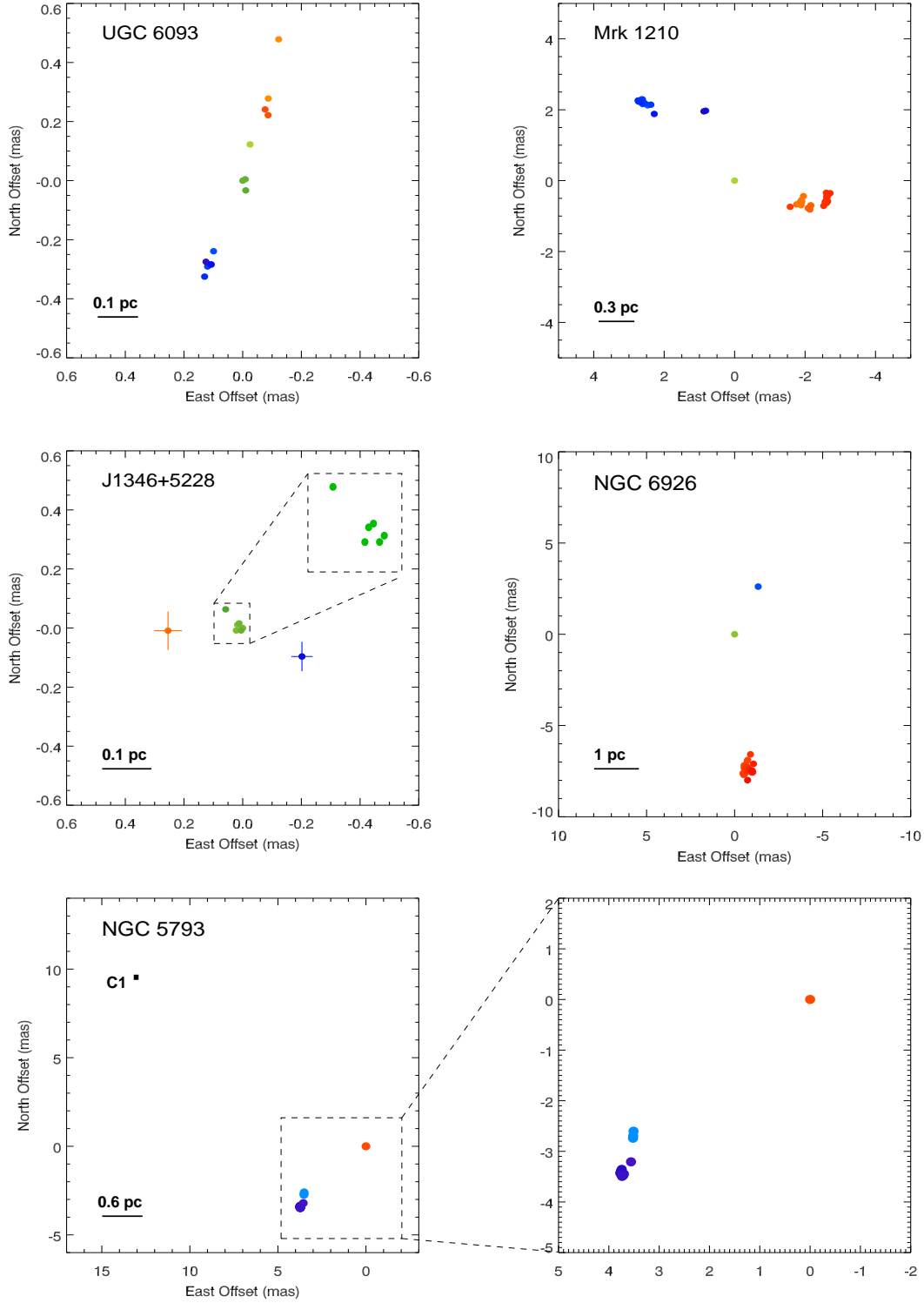


Fig. 3.— VLBI maps of UGC 6093, Mrk 1210, J1346+5228, NGC 6926, and NGC 5793. The data points in the maps are color-coded to indicate redshifted (red), blueshifted (blue), and systemic (green) masers. Except for NGC 5793, each map is centered on the position of the brightest systemic maser. NGC 5793 has no detectable systemic masers, so its map is centered at the brightest redshifted maser feature. A continuum component with SNR  $\sim 5$  which is believed to be a part of the jet component C1 (Hagiwara et al. 2001) was detected  $\sim 20$  mas northeast of the maser emission of NGC 5793 (marked with a black square on the map of NGC 5793).

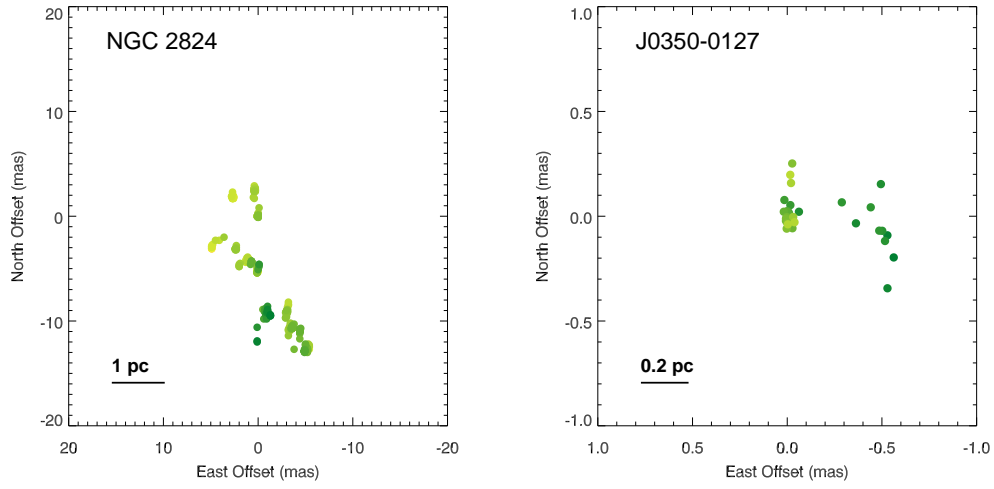


Fig. 4.— VLBI maps of NGC 2824 and J0350–0127. Each map is centered on the position of the brightest maser feature.

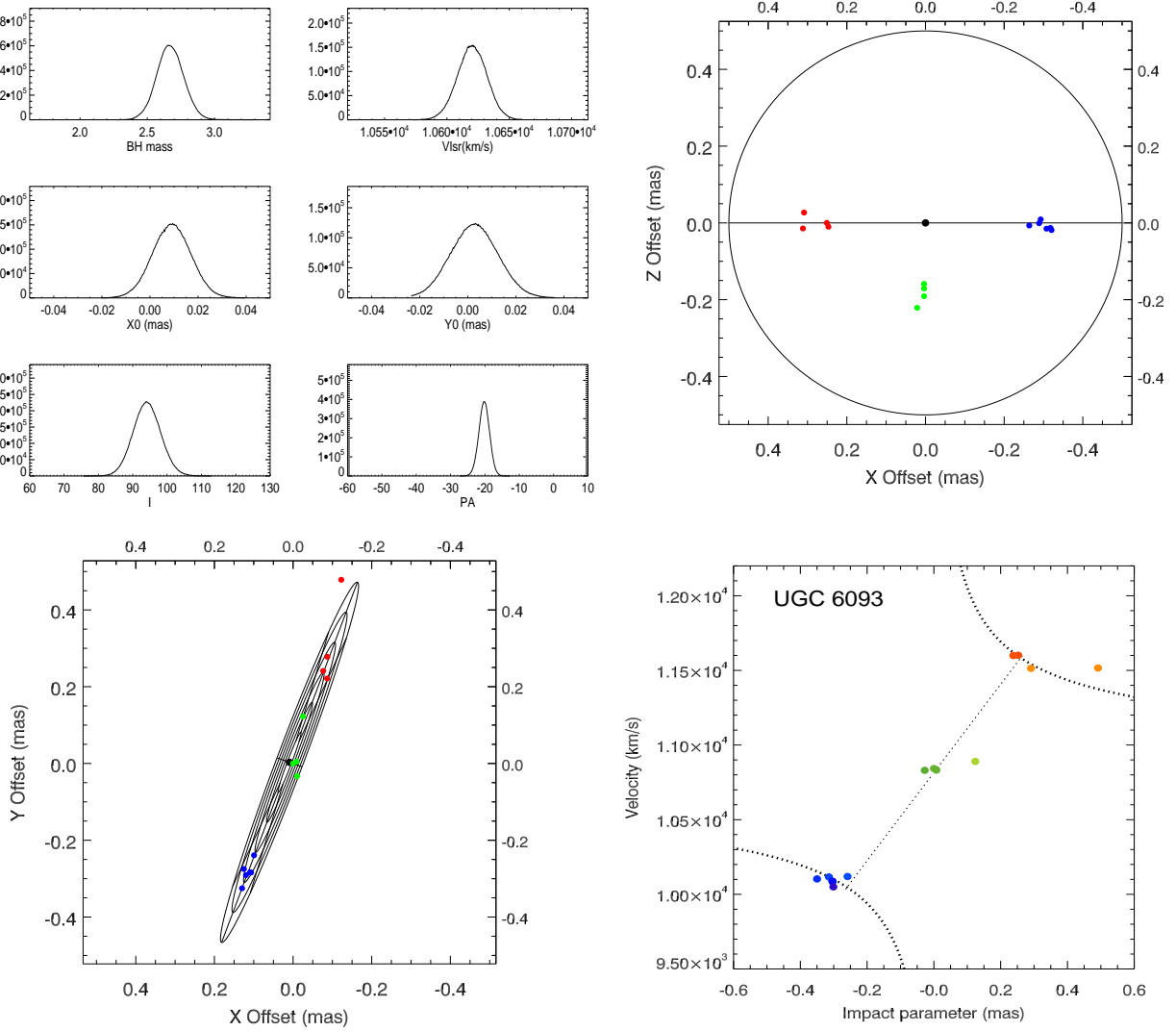


Fig. 5.— Visualization of Bayesian fitting results for UGC 6093. The upper left panel presents the probability density functions (PDFs) of the fitted parameters, while the upper right panel shows a top view of the fitted maser positions. The lower left panel shows the 3-D disk model based on the fitting results overlapping with the observed positions of masers with  $\text{SNR} > 7$ . The lower right panel presents the  $PV$  diagram, and the dash line present the position-velocity relation in an ideal case, an edge-on, flat, Keplerian disk orbiting around a point mass with our fitted value.

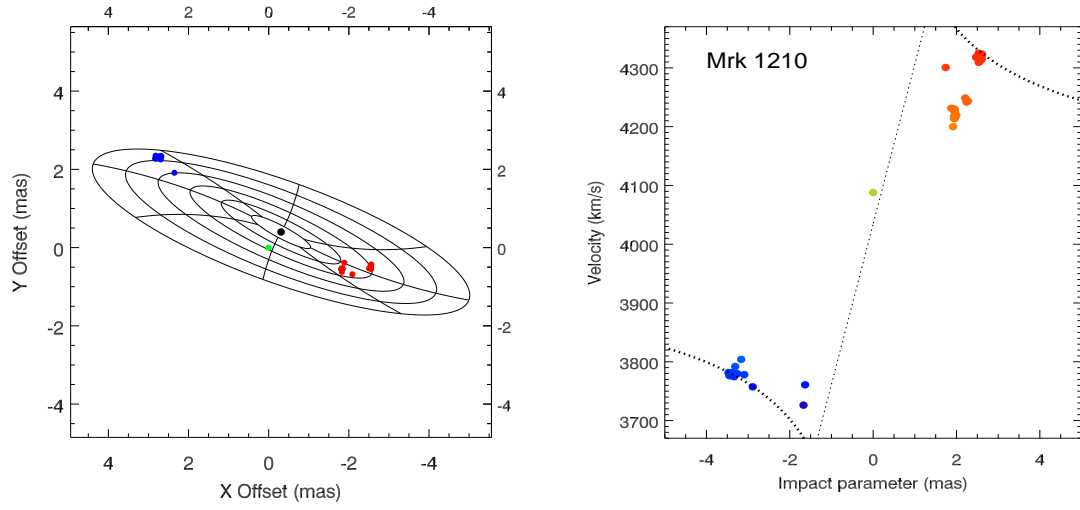


Fig. 6.— The left panel of shows a concept map of a warped and tilted disk overlapping with the observed masers with  $\text{SNR} > 7$  in Mrk 1210. The right panel shows the  $PV$  diagram, in which the dash line presents the  $PV$  relation of an edge-on, flat, Keplerian disk orbiting around a point mass of  $1.42 \times 10^7 M_{\odot}$ .

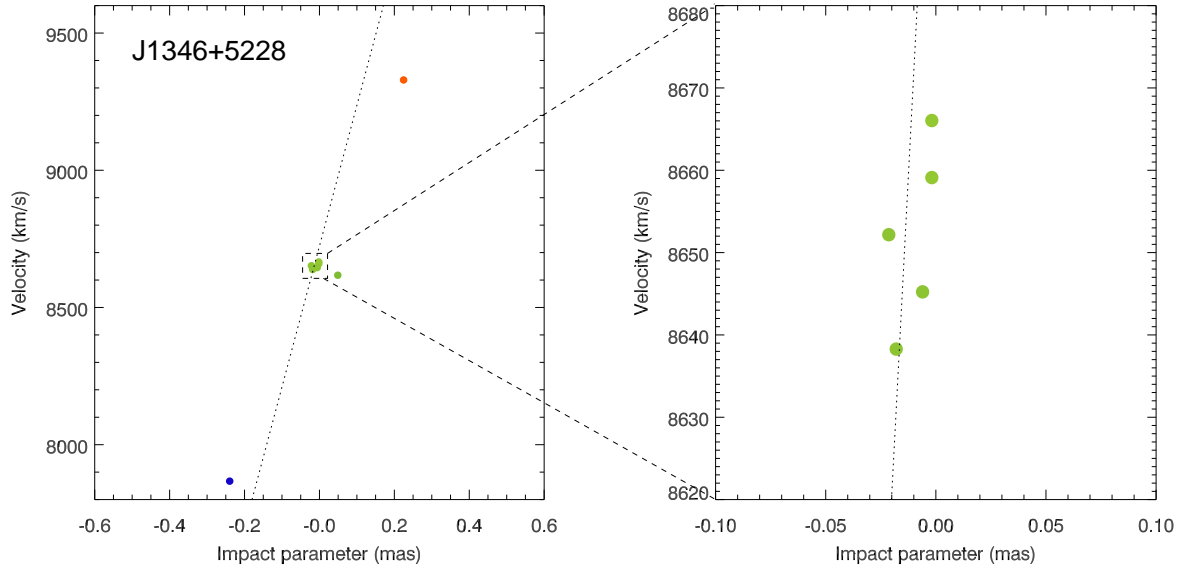


Fig. 7.— Position-Velocity (*PV*) diagram of J1346+5228. The offsets between the positions of masers projected onto the fitted disk plane ( $PA = 77.3^\circ$ ) and the unweighted average position of systemic masers are defined as the “impact parameters”. The distribution of five (out of a total of six) systemic features on the *PV* diagram is consistent with masers at a same radial distance from the dynamical center.